

DiffHash: Text-Guided Targeted Attack via Diffusion Models against Deep Hashing Image Retrieval

Zechao Liu¹, Zheng Zhou¹, Xiangkun Chen¹, Tao Liang¹, Dapeng Lang¹

¹Harbin Engineering University, Harbin 150001, China

{liuzechao, zhouzheng, chenxiangkun, liangtao98, langdapeng}@hrbeu.edu.cn

Abstract

Deep hashing models have been widely adopted to tackle the challenges of large-scale image retrieval. However, these approaches face serious security risks due to their vulnerability to adversarial examples. Despite the increasing exploration of targeted attacks on deep hashing models, existing approaches still suffer from a lack of multimodal guidance, reliance on labeling information and dependence on pixel-level operations for attacks. To address these limitations, we proposed DiffHash, a novel diffusion-based targeted attack for deep hashing. Unlike traditional pixel-based attacks that directly modify specific pixels and lack multimodal guidance, our approach focuses on optimizing the latent representations of images, guided by text information generated by a Large Language Model (LLM) for the target image. Furthermore, we designed a multi-space hash alignment network to align the high-dimension image space and text space to the low-dimension binary hash space. During reconstruction, we also incorporated text-guided attention mechanisms to refine adversarial examples, ensuring them aligned with the target semantics while maintaining visual plausibility. Extensive experiments have demonstrated that our method outperforms state-of-the-art (SOTA) targeted attack methods, achieving better black-box transferability and offering more excellent stability across datasets.

Introduction

The exponential growth of multimedia data on the Internet has posed significant challenges for information retrieval systems. As a solution to information retrieval, hashing (Wang et al. 2017) transforms high-dimensional data to binary codes, enabling efficient large-scale search. This approach offers substantial benefits in storage efficiency and retrieval performance. The rise of deep learning has enhanced traditional hashing methods. Leveraging the powerful feature representation capabilities of deep learning, deep hashing models utilize deep neural networks (DNNs) for automatic feature extraction and have achieved significant success.

The DNN-based deep hashing models, with their powerful feature learning capabilities, have quickly surpassed traditional hashing methods that rely on handcrafted features. However, the deep hashing models inherit the vulnerability of the DNNs, making them susceptible to adversarial examples. Despite much research has focused on the secu-

rity of DNNs like (Szegedy 2013; Kurakin, Goodfellow, and Bengio 2016; Madry 2017; Moosavi-Dezfooli, Fawzi, and Frossard 2016; Brown et al. 2017), fewer studies address the security problems of the deep hashing models. Due to the discretization of deep hashing models, it is more challenging to generate adversarial examples than classifiers or detectors.

Existing attacks on deep hashing models could be divided into targeted attacks (Bai et al. 2020; Wang et al. 2021b, 2023, 2021a; Meng, Chen, and Cao 2024; Zhao et al. 2023; Tang et al. 2024) and untargeted attacks (Lu et al. 2021; Wang, Lin, and Li 2023). In this paper, we focus on targeted attacks, which are more malicious and more challenging to mitigate. Taking online retailers for example, unscrupulous merchants may use targeted attacks on their competitors' products to gain more attention to their own goods, which could cause malignant competition. Compared to the untargeted attack, the targeted attack requires the adversarial examples to be mapped into the preset target hashing codes, which significantly increases the complexity of generating adversarial examples. Although existing methods against deep hashing models have achieved remarkable performance in targeted attacks, they still have several limitations: 1) General methods that rely on structured representation codes and labels often face challenges when dealing with imbalanced datasets and limited label availability for both target and original images. They also lack multimodal semantic guidance, which is vital for effective real-world attacks. 2) Deep hashing models introduce additional complexities for targeted attacks: the non-differentiable sign function causes gradient blockage, while quantization errors arising from binarization lead to reduced semantic accuracy. 3) Most available methods require extensive training for the final attack, which results in expensive resource costs.

To address existing challenges and inspired by recent diffusion-based attacks (Dai, Liang, and Xiao 2025; Chen et al. 2024; Xue et al. 2023), we propose DiffHash, a novel targeted adversarial attack leveraging pre-trained diffusion models against deep hashing. The main contributions are summarized as follows:

- We propose a novel targeted attack method against deep hashing models. To the best of our knowledge, we are the first to transfer targeted attacks into the latent space of diffusion models to address the gradient blockage and

quantization errors in deep hashing. Our latent-space approach enhances robustness and improves attack transferability across deep hashing architectures.

- We leverage LLM-based text representations to guide targeted attacks rather than labels and representation codes. Technically, We propose a multi-space hash alignment operation to unify text and image representations in a shared space, and introduce a network HashAlignNet (HAN) to facilitate this alignment.
- Extensive experiments have demonstrated that the generated adversarial examples are more effective and transferable compared to SOTA targeted attack methods.

Related Work

Deep Hashing Based Image Retrieval

Due to its storage efficiency and retrieval speed, the deep hashing models have become a popular solution for large-scale similarity searches in multimedia applications. Regarding the evolution of the hashing methods, the early techniques were based on hand-crafted approaches, such as Locality-Sensitive Hashing (LSH) (Datar et al. 2004), which focuses on preserving pairwise similarity between data points. With the fast advancement of deep learning, various deep hashing models have been proposed for image retrieval, including HashNet (Cao et al. 2017), DPSH (Li, Wang, and Kang 2016), DCH (Cao et al. 2018a), DAPH (Shen et al. 2017), DPH (Cao et al. 2018b), and CSQ (Yuan et al. 2020).

Adversarial Attacks

Since Szegedy et al. (Szegedy 2013) discovered that small perturbations on images can deceive DNNs and cause misclassifications, adversarial attacks have gained significant attention. As adversarial attack methods continue to evolve, more and more researchers begin to explore the vulnerability of the deep hashing models. Attacks on the deep hashing models can be categorized into two types: targeted attacks and untargeted attacks. Untargeted attack methods include HAG (Yang et al. 2018), AACH (Li et al. 2021), SAA (Lu et al. 2021), CGAT (Wang, Lin, and Li 2023). Targeted attack methods can be divided into two main categories: (1) methods that rely on label-based representation codes and generative models, including GAN-based ProS-GAN (Wang et al. 2021b), THA (Wang et al. 2021a), TUA (Meng, Chen, and Cao 2024), and Diffusion-based HUANG (Huang and Shen 2025); and (2) non-generative methods, such as P2P (Bai et al. 2020), DHTA (Bai et al. 2020), and PTA (Zhao et al. 2023). Among these, PTA is the only gradient-simulating method that does not rely on representation codes or labels.

Diffusion Models and Latent Space

Diffusion models are generative models that progressively denoise random noise to generate high-quality data, offering greater training stability and superior sample quality compared to GANs (Goodfellow et al. 2014) and VAEs (Kingma 2013). It is widely used in image inpainting (Li et al. 2022; Xie et al. 2023), super-resolution (Saharia et al. 2022), and

style transfer (Sun et al. 2024). To address the high computational cost of traditional pixel-space diffusion models like DDPM, Latent Diffusion Models (LDMs) such as Stable Diffusion (Rombach et al. 2022) operate in a compact latent space, significantly reducing complexity and enhancing versatility.

Method

In this section, we will introduce our proposed DiffHash targeted attack method, the overall framework is depicted in Figure 1. DiffHash first encodes all inputs into the latent space of the diffusion model with a *Latent Encoder*. Then the whole process is divided into two stages: in the alignment stage, the encoded latent features are aligned across multiple spaces through the *HashAlignNet*. Subsequently, in the attack stage, the *text guided vector* is employed to optimize the *latent benign image*. Finally, the *Latent Decoder* decodes the optimized *latent benign image* into an *adversarial image*.

Problem Formulation

Given a dataset $\mathcal{D} = \{(x_i, y_i)\}_{i=1}^N$, let N denotes the total number of the images, x_i represents the i -th image and $y_i = [y_{i1}, y_{i2}, \dots, y_{iC}] \in \{0, 1\}^C$ corresponds to a multi-label vector labeled with C classes, where $y_{in} = 1$ indicates the x_i belongs to the n -th class. The semantic similarities between any two images $S_{i,j}$ are defined as

$$S_{i,j} = \begin{cases} 1, & y_i \cap y_j \neq \emptyset \\ 0, & otherwise \end{cases} \quad (1)$$

We consider two images similar if they share at least one common label. A deep hashing model \mathcal{H} maps data (e.g. images) to binary codes and computes the similarities within the database. Generally, given the input image x_i , the deep hashing model will map it to a hash code:

$$b(x_i) = \text{sign}(\mathcal{H}(x_i)), b(x_i) \in \{-1, 1\}^k \quad (2)$$

where $\text{sign}(\cdot)$ represents the sign function, producing binary values in $\{-1, 1\}$, and k is the length of the hash code. To evaluate the similarity between two images x_i and x_j , their respective hash codes $b(x_i)$ and $b(x_j)$ are compared using Hamming distance:

$$d_H(x_i, x_j) = \frac{1}{2} \sum_{l=1}^k |b_l(x_i) - b_l(x_j)| \quad (3)$$

where $b_l(x_i)$ and $b_l(x_j)$ represent l -th bit of hash codes for x_i and x_j .

Multi-Space Hash Alignment

Existing attacks on deep hashing models mostly rely on label information within single-image modalities, restricting their adaptability and effectiveness. We propose a novel targeted attack method that leverages LLM-based textual representations to guide adversarial attacks. To bridge the inherent gap between high-dimensional image and text space, we introduce a Multi-Space Hash Alignment approach which implemented via our HashAlignNet (HAN). HAN comprises

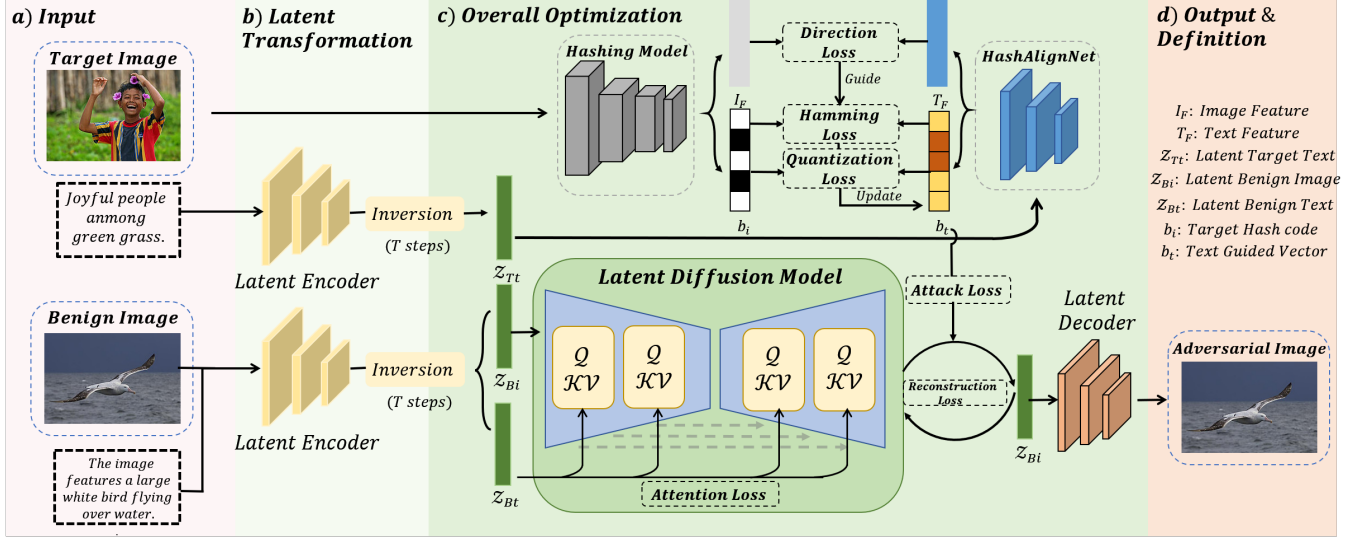


Figure 1: The framework utilizes a latent diffusion model to optimize adversarial examples. Target and benign images with corresponding textual descriptions are encoded into latent representations. They are iteratively refined using multiple loss functions. The optimized latent representations are then decoded to generate adversarial images that effectively achieve targeted attacks on deep hashing models.

three fully connected layers ($1024 \rightarrow 512 \rightarrow 256$). As illustrated in Figure 2, HAN efficiently maps text features into a shared hash space. The input latent target text z_{Tt} , typically derived from a pre-trained text encoder such as Stable Diffusion (Rombach et al. 2022), is projected through HAN into the hash space, yielding text feature T_F and text guided vector b_t .

To ensure the hash representations maintain semantic alignment, we introduce the direction consistency loss \mathcal{L}_{Direct} as:

$$\mathcal{L}_{Direct} = 1 - \frac{1}{N} \sum_{i=1}^N \frac{T_F^{(i)} \cdot I_F^{(i)}}{\|T_F^{(i)}\|_2 \cdot \|I_F^{(i)}\|_2} \quad (4)$$

where we use cosine similarity to control the direction of the alignment, minimize the cosine distance between $T_F^{(i)}$ and $I_F^{(i)}$. The $I_F^{(i)}, T_F^{(i)}$ is the i -th image feature and text feature extracted from the target hash model and HAN. $\|\cdot\|_2$ calculates the L_2 norm of $I_F^{(i)}, T_F^{(i)}$.

However, $b_t^{(i)}$ may inadvertently exceed the binary constraints within the range of -1 to 1 during optimization. To address this issue, we introduce a quantization loss \mathcal{L}_{Quan} as:

$$\mathcal{L}_{Quan} = \frac{1}{N} \sum_{i=1}^N \| |b_t^{(i)}| - 1 \|_2 \quad (5)$$

The text guided vector $b_t^{(i)}$ is generated from i -th textual input by HAN. This loss discourages deviations in the L_2 norm of the textual hash vectors, ensuring that the hash codes remain normalized.

To effectively align textual and visual modalities for robust and precise attacks, we further introduce hamming loss

function \mathcal{L}_{Ham} :

$$\mathcal{L}_{Ham} = \frac{1}{N} \sum_{i=1}^N \|b_t^{(i)} - b(x_i)\|_1 \quad (6)$$

where $b(x_i)$ denotes the corresponding images' hash codes processed by the deep hash model. $\|\cdot\|_1$ calculates the L_1 norm between $b_t^{(i)}$ and $b(x_i)$, thereby encouraging their convergence in the shared hash space. The total loss of hash alignment is defined as:

$$\mathcal{L}_{Align} = \alpha \mathcal{L}_{Direct} + \beta \mathcal{L}_{Quan} + \gamma \mathcal{L}_{Ham} \quad (7)$$

where the α, β, γ are the hyperparameters that weigh the significance of the different losses respectively.

Text-Guided Latent Targeted Attack

In this section, we propose a text-guided targeted attack that operates in the latent space of the diffusion model. Unlike pixel-level attacks like HUANG (Huang and Shen 2025), our approach overcomes two key challenges specific to deep hashing models: (1) the gradient blockage caused by the non-differentiable binarization sign function, (2) quantization errors arising from mapping continuous vectors into discrete binary codes.

Inspired by recent diffusion editing approaches (Couairon et al. 2023; Mokady et al. 2023), we leverage the DDIM Inversion (Song, Meng, and Ermon 2021) to shift the optimization into a latent space. Enabling precise alignment of image latent representations with target semantics. At first, we reverse the benign image into the diffusion latent space:

$$z_{Bi}^0 = Inverse(x_i^{t-1}) = \underbrace{Inverse \circ \dots \circ Inverse(x_i^0)}_t \quad (8)$$

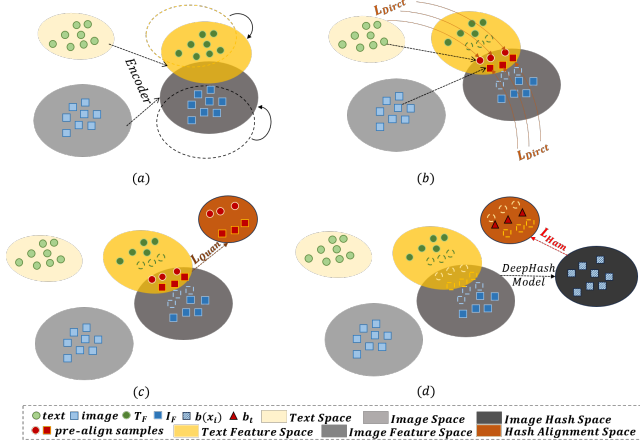


Figure 2: The process of Multi-Space Hash Alignment: (a) text and image samples are first encoded into their feature spaces, (b) then features are brought closer using L_{Direct} , (c) these pre-align samples are quantized into binary codes via L_{Quan} , (d) finally the L_{Ham} further aligns text and image hash codes.

where $Inverse(\cdot)$ denotes the DDIM Inversion operation, we apply this operation for several timesteps let x_i^0 (the benign image) to its latent representation z_{Bi}^0 .

To overcome the gradient blockage limitation, we aim to directly perturb the latent representation z_{Bi}^0 in T steps as:

$$\mathcal{L}_{Distance} = \sum_{t=0}^T \mathcal{J}(b_t, b(z_{Bi}^t); \mathcal{H}) \quad (9)$$

where \mathcal{J} is the cross-entropy loss. z_{Bi}^t denotes the latent vector in the t -th adversarial optimization update. And the b_t is the text-guided vector, which is obtained from HashAlign-Net. To better guide the optimization and manage the quantization errors of the perturbation, we incorporate directional constraints, the loss \mathcal{L}_{Path} are defined as:

$$\begin{aligned} \mathcal{L}_{Path} = & \sum_{t=0}^T \|b_t - b(z_{Bi}^t)\|_1 \\ & + \sum_{t=0}^T \max(0, M_{margin} - (b_t \cdot b(z_{Bi}^t))) \end{aligned} \quad (10)$$

where $\max(0, \cdot)$ ensures that when the dot product $b_t \cdot b(z_{Bi}^t)$ is less than the threshold M_{margin} , the penalty will be triggered to constraint the similarity of the b_t and $b(z_{Bi}^t)$. Finally, the total attack loss combines the $\mathcal{L}_{Distance}$ and \mathcal{L}_{Path} to optimize the adversarial perturbation in the latent space jointly:

$$\mathcal{L}_{Attack} = \mathcal{L}_{Distance} + \mathcal{L}_{Path} \quad (11)$$

Figure 3 shows an example of retrieval results, comparing a benign image with its adversarial example generated by our method.

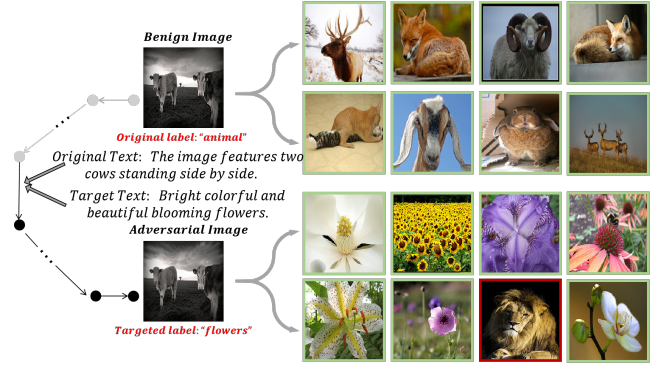


Figure 3: Illustration of the top-8 retrieval results with DiffHash. The adversarial image is generated by the guidance of the targeted text. Images in green/red boxes are the results related/unrelated to the target label.

Optimization and Reconstruction

During denoising iterations, attention maps are aggregated to analyze the model’s focus on image regions relevant to the original text. By leveraging textual guidance derived from the original image, we constrain deviations in attention distribution through variance minimization. This approach ensures semantic coherence and maintains consistent attention to textually relevant regions throughout the optimization process. This is mathematically represented as:

$$\mathcal{L}_{Attention} = \frac{1}{H \times W \times S} \sum_{s=1}^S \sum_{h=1}^H \sum_{w=1}^W (\mathcal{A}_{h,w}^s(z_{Bt}) - \mu_s)^2 \quad (12)$$

where $\mathcal{A}_{h,w}^s$ denotes the attention value at location (h, w) for the s -th attention head, S is the number of attention heads, H and W are the spatial dimensions of the attention map, μ_s is the mean attention value for the s -th attention head. z_{Bt} represents the latent benign text vector, which provides semantic guidance to the attention mechanism.

To ensure perceptual quality while achieving the adversarial objective, we add reconstruction loss to guide the optimization. It enforces latent-level consistency, promote smoothness preserving both low-level details and high-level features between the original and adversarial images. This is mathematically represented as:

$$\begin{aligned} \mathcal{L}_{Recon} = & \frac{1}{H_z \times W_z} \sum_{i=1}^{H_z} \sum_{j=1}^{W_z} [(z_{Bi}^0(i, j) - z_{Bi}^t(i, j))^2 \\ & + (z_{Bi}^t(i+1, j) - z_{Bi}^t(i, j))^2 + (z_{Bi}^t(i, j+1) - z_{Bi}^t(i, j))^2] \end{aligned} \quad (13)$$

where H_z and W_z denote the height and width of the latent vector, while $i \in \{1, \dots, H_z\}$ and $j \in \{1, \dots, W_z\}$ index its spatial coordinates. The $z_{Bi}^0(i, j)$ refers to the latent value at location (i, j) for the original image. Finally, our whole optimization goal could be defined as:

$$\argmin \quad \kappa_1 \cdot \mathcal{L}_{Attack} + \kappa_2 \cdot \mathcal{L}_{Recon} + \kappa_3 \cdot \mathcal{L}_{Attention} \quad (14)$$

The outline of DiffHash is shown in Algorithm 1.

Method	Metric	NUS-WIDE			FLICKR-25K			MS-COCO		
		16 bits	32 bits	64 bits	16 bits	32 bits	64 bits	16 bits	32 bits	64 bits
Original	t-MAP	27.38	26.70	25.52	43.52	42.82	42.82	24.01	21.69	20.15
P2P	t-MAP	39.39	35.88	42.49	59.86	57.15	52.41	30.97	29.56	28.87
DHTA	t-MAP	39.98	36.13	43.34	50.93	52.36	52.13	30.82	29.50	29.09
ProS-GAN	t-MAP	67.01	74.31	69.37	63.41	60.99	57.60	34.67	<u>55.71</u>	50.21
THA	t-MAP	60.65	<u>75.77</u>	<u>74.63</u>	66.69	60.31	<u>60.44</u>	38.95	51.71	32.51
PTA	t-MAP	71.31	72.59	71.64	47.02	55.61	54.23	<u>57.49</u>	52.76	<u>60.24</u>
HUANG	t-MAP	57.12	58.61	63.55	60.22	<u>61.15</u>	59.43	48.16	49.36	50.44
DiffHash (Ours)	t-MAP	<u>69.13</u>	79.97	77.62	<u>65.32</u>	62.67	61.33	62.46	59.42	61.49

Table 1: t-MAP@5000 of different targeted adversarial attack methods with 16,32 and 64 hash bits on three datasets. The best results are highlighted in bold, while the second-best results are underlined.

Algorithm 1: DiffHash Targeted Attack

Input: Clean query image x , latent benign text z_{Bt} , target image x_t , latent target text z_{Tt} , Diffusion model \mathcal{M} , Deep hashing model \mathcal{H} , HashAlignNet f_{HAN} , Loss weights: $\kappa_1, \kappa_2, \kappa_3$, Total inversion steps T , learning rate η

Output: Adversarial image x'

- 1: Obtain latent representation from x_i^{t-1} :
 $z_{Bi}^0 = \text{Inverse}(x_i^{t-1}) = \text{Inverse} \circ \dots \circ \text{Inverse}(x_i^0)$
- 2: $(T_F, b_t) \leftarrow f_{\text{HAN}}(z_{Tt})$
- 3: $(I_F, b_{Bt}) \leftarrow f_{\text{HAN}}(z_{Bt})$
- 4: **for** $t = 1$ to T **do**
- 5: $z_{Bi}^t \leftarrow \text{diffusion_step}(\mathcal{M}, z_{Bi}^{t-1}, z_{Bt}, t)$
- 6: $\arg \min \mathcal{L}_{\text{Total}} = \kappa_1 \cdot \mathcal{L}_{\text{Attack}}(b_t, b(z_{Bi}^t)) + \kappa_2 \cdot \mathcal{L}_{\text{Recon}}(z_{Bi}^0, z_{Bi}^t) + \kappa_3 \cdot \mathcal{L}_{\text{Attention}}(z_{Bt})$.
where $b(z_{Bi}^t) = f_{\text{HAN}}(z_{Bi}^t)$.
- 7: $z_{Bi}^t \leftarrow z_{Bi}^t - \eta \nabla (\mathcal{L}_{\text{Total}}(z_{Bi}^t, z_{Bt}, z_{Bi}^0))$
- 8: **end for**
- 9: $x' \leftarrow \text{Decode}(\mathcal{M}, z_{Bi}^T)$
- 10: **Output:** Adversarial image x' .

Experiment

Experiment Setup and Preparation

Following (Zhao et al. 2023), we evaluate our method on three multi-label datasets: FLICKR-25K (38 labels, 1,900 query/target images)(Huiskes and Lew 2008), NUS-WIDE (21 labels, 2,100 query/target images)(Chua et al. 2009), and MS-COCO (80 labels, 1,800 query/target images) (Lin et al. 2014), each with 5,000 images randomly selected for hash alignment. For consistency, we use an LLM (e.g., Fuyu-8B (AI 2023)) using the prompt: *Write a simple five-sentence description of this image.* to generate five descriptions per image, filtering out descriptions with low CLIP similarity (< 0.25) (Radford et al. 2021). We evaluate targeted attack effectiveness using target mean average precision (t-MAP) on the top 5,000 retrieved images from the database following (Zhao et al. 2023). Higher t-MAP scores indicate better attack performance.

Baselines. Following (Zhao et al. 2023), we use CSQ (Yuan et al. 2020) with a ResNet-50 backbone as the base-

line hashing model. We compare our DiffHash against SOTA targeted attack methods: P2P (Bai et al. 2020), DHTA (Bai et al. 2020), PTA (Zhao et al. 2023), Pros-Gan (Wang et al. 2021b), THA (Wang et al. 2021a), and HUANG (Huang and Shen 2025), with perturbation constraint $\epsilon = 8/255$.

Implementation Details. We employ pre-trained *Stable Diffusion v2-base* with DDIM sampling (Song, Meng, and Ermon 2021). Optimization uses AdamW ($lr = 1e^{-3}$, 30 iterations) (Loshchilov 2017). Experiments are conducted on an NVIDIA RTX 4090D GPU, where DiffHash generates adversarial examples with 16.59 GB of GPU memory.

Results and Analysis

We evaluated the t-MAP@5000 of DiffHash against six SOTA methods across three datasets (Table 1). DiffHash consistently achieves competitive or superior performance compared to baselines. On MS-COCO, DiffHash notably surpasses ProS-GAN by 27.79% (16-bit) and PTA by 6.66% (32-bit). On FLICKR-25K, it closely following THA by only 1.37% at 16-bit and outperforming baselines in longer hash lengths. On NUS-WIDE, DiffHash particularly excels at 32-bit and 64-bit settings by surpassing PTA and ProS-GAN, although it slightly trails PTA by 2.18% at the 16-bit setting. Compared to another diffusion-based method HUANG (Huang and Shen 2025), DiffHash achieves improvements ranging from 10.93% to 21.36% on NUS-WIDE, 1.52% to 5.10% on FLICKR-25K, and 11.05% to 14.30% on MS-COCO.

The improved performance of DiffHash mainly comes from its text-guided optimization, which effectively captures more semantic details than label-based methods, especially helpful for large-category datasets like MS-COCO. However, slightly weaker performance observed in shorter hash codes (16-bit on NUS-WIDE and FLICKR-25K) reflects the inherent difficulty in retaining detailed semantic information within limited hash lengths.

Figure 4 shows that DiffHash yields consistently high t-MAP scores. On FLICKR-25K and MS-COCO most values lie between 0.5 and 0.9, while on NUS-WIDE over 80 % of queries exceed 0.9, underscoring its stable and superior targeted-attack performance across bit lengths.

Method	Metric	NUS-WIDE			FLICKR-25K			MS-COCO		
		DPH	HashNet	DPSH	DPH	HashNet	DPSH	DPH	HashNet	DPSH
Original	t-MAP	54.03	61.98	65.34	38.81	43.06	47.70	17.35	24.11	29.59
P2P	t-MAP	46.11	53.30	56.33	35.64	38.94	47.50	14.65	24.39	31.53
DHTA	t-MAP	56.76	54.17	57.43	40.33	43.83	52.01	15.24	26.23	34.38
ProS-GAN	t-MAP	60.55	63.77	66.37	39.19	43.72	44.66	22.53	23.76	39.79
THA	t-MAP	60.78	63.41	71.25	35.22	40.34	38.72	19.48	23.97	28.52
PTA	t-MAP	<u>60.91</u>	60.44	60.85	46.58	52.13	62.55	24.43	29.26	42.05
HUANG	t-MAP	60.05	56.11	63.49	<u>55.26</u>	<u>54.61</u>	56.94	<u>43.11</u>	<u>42.91</u>	<u>49.50</u>
DiffHash	t-MAP	61.11	64.21	<u>67.19</u>	57.04	60.49	<u>59.09</u>	60.17	53.39	52.22

Table 2: Performance comparison of different methods across three datasets using three hashing models (DPH, HashNet, DPSH) with ResNet-50 backbone and 32-bit hash length.

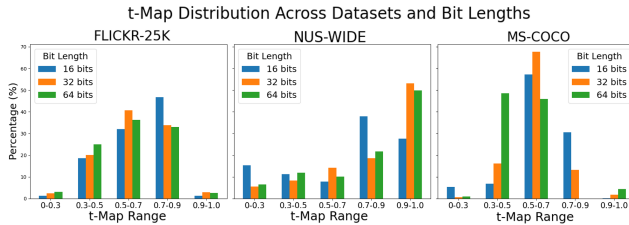


Figure 4: The distribution of t-MAP across three datasets and hash bit lengths (16, 32, 64).

Universality Across Hashing Methods

As shown in Table 2, we evaluated the generalization of DiffHash using 32-bit hash codes across multiple hashing methods (DPH, DPSH, HashNet) with a ResNet-50 backbone. DiffHash consistently outperforms SOTA methods across datasets, maintaining approximately 60% t-MAP across NUS-WIDE, FLICKR-25K, and MS-COCO. As the number of dataset labels increases, methods like THA and ProS-GAN experience significant performance drops, with reductions of over 15% relative to FLICKR-25K and 30% compared to NUS-WIDE. Meanwhile, PTA and HUANG also show some decrease which highlights baseline’s reliance on label information. Although HUANG performs competitively on MS-COCO, DiffHash consistently outperforms HUANG across all datasets. However, DiffHash slightly lower t-MAP on DPSH for NUS-WIDE and FLICKR-25K can be primarily attributed to DPSH’s heavy reliance on pairwise similarity, which limits effective exploitation of the richer semantic consistency available in textual data.

Black-box Transferability

As shown in Table 3, DiffHash demonstrates improved black-box transferability compared to other SOTA methods on other backbones. Our DiffHash outperforms PTA by nearly 19% and consistently beating HUANG on every architecture. This superior performance can be attributed to the use of rich semantic text information from the target image, in contrast to other approaches that rely solely on label information.

Method	Backbone Networks				
	ResNet-18	ResNet-101	VGG-11	VGG-16	AlexNet
Clean	8.55	7.93	7.71	6.74	8.65
P2P	10.13	9.69	9.79	9.43	10.20
DHTA	11.09	10.57	12.16	10.70	12.11
ProS-GAN	<u>49.12</u>	45.23	42.21	45.24	43.36
THA	38.95	36.64	33.34	37.40	35.20
PTA	48.58	<u>46.46</u>	45.34	45.48	42.19
HUANG	34.13	<u>42.66</u>	<u>51.37</u>	<u>49.28</u>	<u>50.46</u>
Ours	65.34	65.11	67.34	61.13	62.24

Table 3: Performance comparison of different methods across five backbone networks.

Time Efficiency Analysis and Visual Comparison

Regarding efficiency, we compared DiffHash with generative attack methods on the NUS-WIDE dataset as shown in Table 4. DiffHash significantly outperforms GAN-based methods like ProS-GAN and THA by eliminating the need for extensive training. Moreover, operating in the latent space, DiffHash achieves faster processing per image compared to HUANG.

Method	Training Time (s)	Per(s)
ProS-GAN	36,031	0.06
THA	35,544	0.05
HUANG	-	30.11
Ours	-	19.52

Table 4: Time efficiency comparison of different generative methods on NUS-WIDE.

As shown in Figure 5, to evaluate the imperceptibility of DiffHash, we visually compared adversarial examples generated by DiffHash and other SOTA methods. Although methods like DHTA and P2P generate subtle perturbations, their t-MAP remains relatively low. Generative methods like ProS-GAN and THA achieve higher t-MAP but produce noticeable artifacts and visible perturbations. PTA similarly introduces obvious perturbations, whereas HUANG pro-

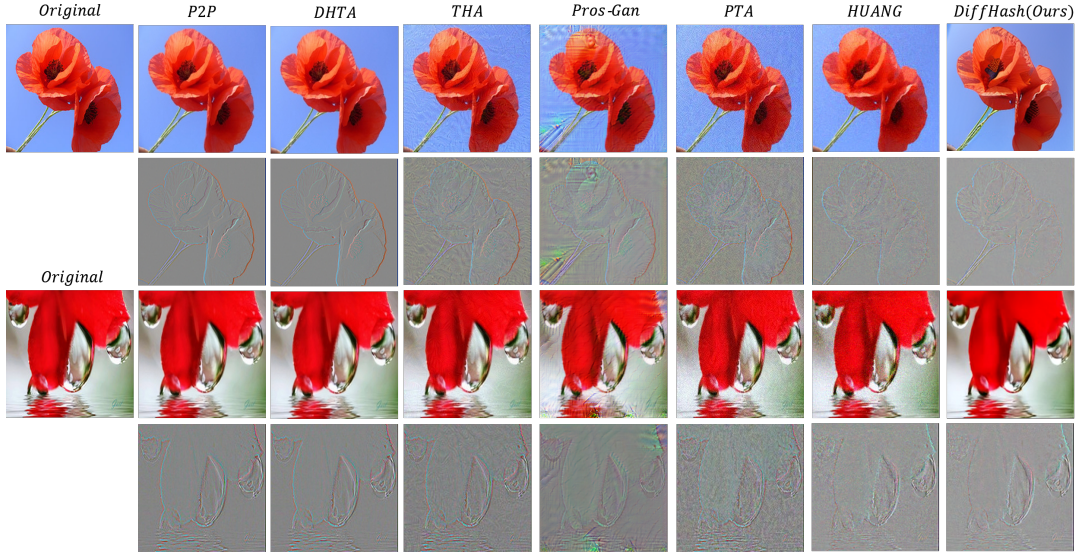


Figure 5: Visual comparison of adversarial examples and perturbation generated by different methods in NUS-WIDE under the same baseline.

duces smoother images but still displays distortion and blurring. In contrast, DiffHash performs optimization in a low-dimensional, semantically meaningful latent space, enabling highly precise and subtle perturbations, clearly demonstrated in the perturbation visualizations. Thus, DiffHash achieves superior imperceptibility while maintaining effective attack performance.

Method	Hyperparameters			t-MAP (%)
	κ_1	κ_2	κ_3	
κ_1 Only	15	0	0	42.35
κ_1 Only w/o HAN	15	0	0	12.63
κ_2 Only	0	1	0	1.67
κ_2 Only w/o HAN	0	1	0	0
κ_3 Only	0	0	8	1.67
κ_3 Only w/o HAN	0	0	8	0
κ_1 and κ_2	15	1	0	59.45
κ_1 and κ_2 w/o HAN	15	1	0	11.79
κ_2 and κ_3	0	1	8	0
κ_2 and κ_3 w/o HAN	0	1	8	0
κ_1 and κ_3	15	0	8	66.80
κ_1 and κ_3 w/o HAN	15	0	8	14.11
$\kappa_1 + \kappa_2 + \kappa_3$	15	1	8	82.10
$\kappa_1 + \kappa_2 + \kappa_3$ w/o HAN	15	1	8	22.16

Table 5: Ablation study on the influence of different settings on t-MAP.

Ablation Study

Table 5 and Figure 6 illustrate the effects of different settings and the presence of HAN on attack performance and visual quality. Specifically, w/o HAN means that HAN has

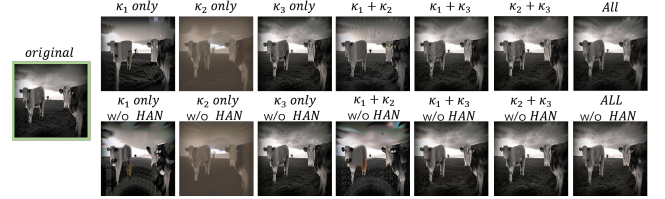


Figure 6: Visual comparison of adversarial examples under different hyperparameter settings.

been removed. Using individual loss functions alone yields poor results, both quantitatively (low t-MAP scores) and visually (noticeable distortions). Combining two losses improves performance moderately. However, the best results are achieved when integrating all three losses with HAN. Notably, omitting HAN significantly reduces performance across all settings, underscoring its essential role in feature alignment.

Conclusion

In this work, we proposed DiffHash, a novel approach for generating targeted adversarial attacks on deep hashing models by optimizing in the latent space of diffusion model. Unlike traditional methods that rely on label information, DiffHash leverages text guidance to ensure robust attacks. Additionally, we achieved multi-space hash alignment by HAN. Our approach demonstrates significant improvements in black-box transferability and stability across multiple datasets. Extensive experiments show that DiffHash outperforms SOTA methods in terms of both attack effectiveness and visual quality. We hope this work inspires further research into the security of image retrieval models.

References

- AI, A. 2023. Fuyu-8B: A multimodal architecture for AI agents.
- Bai, J.; Chen, B.; Li, Y.; Wu, D.; Guo, W.; Xia, S.-T.; and Yang, E.-H. 2020. Targeted Attack for Deep Hashing Based Retrieval. In *European Conference on Computer Vision (ECCV)*, 618–634.
- Brown, T. B.; Mané, D.; Roy, A.; Abadi, M.; and Gilmer, J. 2017. Adversarial patch. *arXiv preprint arXiv:1712.09665*.
- Cao, Y.; Long, M.; Liu, B.; and Wang, J. 2018a. Deep cauchy hashing for hamming space retrieval. In *Proceedings of the IEEE conference on computer vision and pattern recognition (CVPR)*, 1229–1237.
- Cao, Z.; Long, M.; Wang, J.; and Yu, P. S. 2017. Hashnet: Deep learning to hash by continuation. In *Proceedings of the IEEE international conference on computer vision (ICCV)*, 5608–5617.
- Cao, Z.; Sun, Z.; Long, M.; Wang, J.; and Yu, P. S. 2018b. Deep priority hashing. In *Proceedings of the 26th ACM international conference on Multimedia (ACM MM)*, 1653–1661.
- Chen, J.; Chen, H.; Chen, K.; Zhang, Y.; Zou, Z.; and Shi, Z. 2024. Diffusion models for imperceptible and transferable adversarial attack. *IEEE Transactions on Pattern Analysis and Machine Intelligence (TPAMI)*.
- Chua, T.-S.; Tang, J.; Hong, R.; Li, H.; Luo, Z.; and Zheng, Y. 2009. Nus-wide: a real-world web image database from national university of singapore. In *Proceedings of the ACM international conference on image and video retrieval (CIVR)*, 1–9.
- Couairon, G.; Verbeek, J.; Schwenk, H.; and Cord, M. 2023. DiffEdit: Diffusion-based Semantic Image Editing with Mask Guidance. In *International Conference on Learning Representations (ICLR)*.
- Dai, X.; Liang, K.; and Xiao, B. 2025. Advdiff: Generating unrestricted adversarial examples using diffusion models. In *European Conference on Computer Vision (ECCV)*, 93–109. Springer.
- Datar, M.; Immorlica, N.; Indyk, P.; and Mirrokni, V. S. 2004. Locality-sensitive hashing scheme based on p-stable distributions. In *Proceedings of the twentieth annual symposium on Computational geometry (SoCG)*, 253–262.
- Goodfellow, I.; Pouget-Abadie, J.; Mirza, M.; Xu, B.; Warde-Farley, D.; Ozair, S.; Courville, A.; and Bengio, Y. 2014. Generative adversarial nets. *Advances in neural information processing systems (NeurIPS)*.
- Huang, C.; and Shen, X. 2025. HUANG: A Robust Diffusion Model-based Targeted Adversarial Attack Against Deep Hashing Retrieval. In *Proceedings of the AAAI Conference on Artificial Intelligence (AAAI)*, 3626–3634.
- Huiskes, M. J.; and Lew, M. S. 2008. The mir flickr retrieval evaluation. In *Proceedings of the 1st ACM international conference on Multimedia information retrieval*, 39–43.
- Kingma, D. P. 2013. Auto-encoding variational bayes. *arXiv preprint arXiv:1312.6114*.
- Kurakin, A.; Goodfellow, I.; and Bengio, S. 2016. Adversarial machine learning at scale.
- Li, C.; Gao, S.; Deng, C.; Liu, W.; and Huang, H. 2021. Adversarial attack on deep cross-modal hamming retrieval. In *Proceedings of the IEEE/CVF International Conference on Computer Vision (ICCV)*.
- Li, W.; Lin, Z.; Zhou, K.; Qi, L.; Wang, Y.; and Jia, J. 2022. Mat: Mask-aware transformer for large hole image inpainting. In *Proceedings of the IEEE/CVF conference on computer vision and pattern recognition (CVPR)*, 10758–10768.
- Li, W.-J.; Wang, S.; and Kang, W.-C. 2016. Feature learning based deep supervised hashing with pairwise labels. In *Proceedings of the Twenty-Fifth International Joint Conference on Artificial Intelligence (IJCAI)*, 1711–1717.
- Lin, T.-Y.; Maire, M.; Belongie, S.; Hays, J.; Perona, P.; Ramanan, D.; Dollár, P.; and Zitnick, C. L. 2014. Microsoft coco: Common objects in context. In *European Conference on Computer Vision (ECCV)*, 740–755. Springer.
- Loshchilov, I. 2017. Decoupled weight decay regularization. *arXiv preprint arXiv:1711.05101*.
- Lu, J.; Chen, M.; Sun, Y.; Wang, W.; Wang, Y.; and Yang, X. 2021. A smart adversarial attack on deep hashing based image retrieval. In *Proceedings of the 2021 international conference on multimedia retrieval (ICMR)*, 227–235.
- Madry, A. 2017. Towards deep learning models resistant to adversarial attacks.
- Meng, F.; Chen, X.; and Cao, Y. 2024. Targeted Universal Adversarial Attack on Deep Hash Networks. In *Proceedings of the 2024 International Conference on Multimedia Retrieval (ICMR)*, 165–174.
- Mokady, R.; Hertz, A.; Aberman, K.; Pritch, Y.; and Cohen-Or, D. 2023. Null-text inversion for editing real images using guided diffusion models. In *Proceedings of the IEEE/CVF Conference on Computer Vision and Pattern Recognition (CVPR)*, 6038–6047.
- Moosavi-Dezfooli, S.-M.; Fawzi, A.; and Frossard, P. 2016. Deepfool: a simple and accurate method to fool deep neural networks. In *Proceedings of the IEEE conference on computer vision and pattern recognition (CVPR)*, 2574–2582.
- Radford, A.; Kim, J. W.; Hallacy, C.; Ramesh, A.; Goh, G.; Agarwal, S.; Sastry, G.; Askell, A.; Mishkin, P.; Clark, J.; et al. 2021. Learning transferable visual models from natural language supervision. In *International conference on machine learning (ICML)*, 8748–8763.
- Rombach, R.; Blattmann, A.; Lorenz, D.; Esser, P.; and Ommer, B. 2022. High-resolution image synthesis with latent diffusion models. In *Proceedings of the IEEE/CVF conference on computer vision and pattern recognition (CVPR)*, 10684–10695.
- Saharia, C.; Ho, J.; Chan, W.; Salimans, T.; Fleet, D. J.; and Norouzi, M. 2022. Image super-resolution via iterative refinement. *IEEE transactions on pattern analysis and machine intelligence (TPAMI)*, 4713–4726.
- Shen, F.; Gao, X.; Liu, L.; Yang, Y.; and Shen, H. T. 2017. Deep asymmetric pairwise hashing. In *Proceedings of the 25th ACM international conference on Multimedia (ACM MM)*, 1522–1530.

Song, J.; Meng, C.; and Ermon, S. 2021. Denoising Diffusion Implicit Models. In *International Conference on Learning Representations (ICLR)*.

Sun, Y.; Yu, L.; Xie, H.; Li, J.; and Zhang, Y. 2024. DiffAM: Diffusion-based Adversarial Makeup Transfer for Facial Privacy Protection. In *Proceedings of the IEEE/CVF Conference on Computer Vision and Pattern Recognition (CVPR)*, 24584–24594.

Szegedy, C. 2013. Intriguing properties of neural networks.

Tang, L.; Ye, D.; Lv, Y.; Chen, C.; and Zhang, Y. 2024. Once and for All: Universal Transferable Adversarial Perturbation against Deep Hashing-Based Facial Image Retrieval. In *Proceedings of the AAAI Conference on Artificial Intelligence (AAAI)*, 5136–5144.

Wang, J.; Zhang, T.; Sebe, N.; Shen, H. T.; et al. 2017. A survey on learning to hash. *IEEE transactions on pattern analysis and machine intelligence (TPAMI)*, 769–790.

Wang, T.; Zhu, L.; Zhang, Z.; Zhang, H.; and Han, J. 2023. Targeted adversarial attack against deep cross-modal hashing retrieval. *IEEE Transactions on Circuits and Systems for Video Technology (TCSVT)*, 6159–6172.

Wang, X.; Lin, Y.; and Li, X. 2023. Cgat: Center-guided adversarial training for deep hashing-based retrieval. In *Proceedings of the ACM web conference (WWW)*, 3268–3277.

Wang, X.; Zhang, Z.; Lu, G.; and Xu, Y. 2021a. Targeted attack and defense for deep hashing. In *Proceedings of the 44th International ACM SIGIR Conference on Research and Development in Information Retrieval (SIGIR)*, 2298–2302.

Wang, X.; Zhang, Z.; Wu, B.; Shen, F.; and Lu, G. 2021b. Prototype-supervised adversarial network for targeted attack of deep hashing. In *Proceedings of the IEEE/CVF conference on computer vision and pattern recognition (CVPR)*, 16357–16366.

Xie, S.; Zhang, Z.; Lin, Z.; Hinz, T.; and Zhang, K. 2023. Smartbrush: Text and shape guided object inpainting with diffusion model. In *Proceedings of the IEEE/CVF Conference on Computer Vision and Pattern Recognition (CVPR)*, 22428–22437.

Xue, H.; Araujo, A.; Hu, B.; and Chen, Y. 2023. Diffusion-based adversarial sample generation for improved stealthiness and controllability. *Advances in Neural Information Processing Systems (NeurIPS)*, 2894–2921.

Yang, E.; Liu, T.; Deng, C.; and Tao, D. 2018. Adversarial examples for hamming space search. *IEEE transactions on cybernetics*.

Yuan, L.; Wang, T.; Zhang, X.; Tay, F. E.; Jie, Z.; Liu, W.; and Feng, J. 2020. Central similarity quantization for efficient image and video retrieval. In *Proceedings of the IEEE/CVF conference on computer vision and pattern recognition (CVPR)*, 3083–3092.

Zhao, W.; Song, J.; Yuan, S.; Gao, L.; Yang, Y.; and Shen, H. 2023. Precise Target-Oriented Attack against Deep Hashing-based Retrieval. In *Proceedings of the 31st ACM International Conference on Multimedia (ACM MM)*, 6379–6389.